Analyst

RSC Publishing

PAPER

A tyrosinase biosensor based on ordered mesoporous carbon–Au/L-lysine/Au nanoparticles for simultaneous determination of hydroquinone and catechol†

Cite this: *Analyst*, 2013, **138**, 3552

Lin Tang,*[ab] Yaoyu Zhou,[ab] Guangming Zeng,*[ab] Zhen Li,[ab] Yuanyuan Liu,[ab] Yi Zhang,[ab] Guiqiu Chen,[ab] Guide Yang,[ab] Xiaoxia Lei[ab] and Mengshi Wu[ab]

A novel biosensor was developed based on tyrosinase immobilization with ordered mesoporous carbon–Au (OMC–Au), L-lysine membrane and Au nanoparticles on a glassy carbon electrode (GCE). It was applied for the simultaneous determination of dihydroxybenzene isomers using differential pulse voltammetry (DPV). The tyrosinase/OMC–Au/L-lysine/Au film was characterized by scanning electron microscopy (SEM) and impedance spectra. Under optimized conditions, the DPV study results for two isomers, hydroquinone (HQ, 1,4-dihydroxybenzene) and catechol (CC, 1,2-dihydroxybenzene) showed low peak potentials, and the peak-to-peak difference was about 135.85 mV, which ensured the anti-interference ability of the biosensor and made simultaneous detection of dihydroxybenzene isomers possible in real samples. DPV peak currents increased linearly with concentration over the range of 4.0×10^{-7} to 8.0×10^{-5} M, and the detection limits of hydroquinone and catechol were 5×10^{-8} M and 2.5×10^{-8} M ($S/N = 3$), respectively. The tyrosinase biosensor exhibited good repeatability and stability. In addition, the response mechanism of enzyme catalysed redox on the OMC–Au/L-lysine/Au film modified electrode based on electrochemical study was discussed. The proposed method could be extended for the development of other enzyme-based biosensors.

Received 31st December 2012
Accepted 2nd April 2013

DOI: 10.1039/c3an36928e

www.rsc.org/analyst

Introduction

Hydroquinone and catechol are two isomers of phenolic compounds, and have been widely used in cosmetics, tanning, pesticides, flavoring agents, medicines, dye and photography chemicals.[1] These compounds are considered to be significant airborne toxic environmental pollutants. Due to their high toxicity and low degradability in the ecological environment, they are harmful to human health and environment.[2] It is a challenge to directly determine the isomers simultaneously because of their similar structures and properties. So far, a great number of methods have been used for their determination, such as high performance liquid chromatography,[3] pH based-flow injection analysis,[4] synchronous fluorescence,[5] spectrophotometry,[6] electrochemical methods,[7] *etc.* However, these aforementioned methods have the disadvantages of being time-consuming, having expensive instrumentation, low sensitivity, complicated pretreatment procedures and a requirement for professional operators. On the contrary, biosensors are considered as suitable complementary tools for real-time detection of CC and HQ in real samples.

Tyrosinase is a binuclear copper containing metalloprotein (EC 1.14.18.1) that catalyzes oxidation of diphenols to *o*-quinones and hydroxylation of monophenols into diphenols.[8] The analytical role of tyrosinase in biosensor terms was first reported by Macholan and Schanel, who measured the reduction of oxygen in the determination of phenolic substrates.[9] Since then, tyrosinase based biosensors have attracted significant attention in the monitoring of phenols,[10–12] such as catechol, *p*-cresol and phenol. To the best of our knowledge a tyrosinase biosensor for the simultaneous determination of CC and HQ has not yet been reported. The reason for this may be that researchers have regularly evaluated the biosensor by amperometry, without the use of differential pulse voltammetry (DPV), while hydroquinone can only act as secondary substrate of tyrosinase when catechol is available as occurs in the tyrosinase-catalysed redox reaction.[13] The amperometry method tests the two substances at each reduction potential separately, and the DPV method can detect the two substances with redox reactions combined.

The key point lies in the immobilization procedure of tyrosinase on the sensor surface. The quality of the electron transfer between the enzyme redox center and the electrode can be significantly enhanced by using conductive nano-porous-structured materials.[14] Recently, OMCs have received

[a]*College of Environmental Science and Engineering, Hunan University, Changsha, 410082, PR China. E-mail: tanglin@hnu.edu.cn; zgming@hnu.edu.cn; Fax: +86-731-88822778; Tel: +86-731-88822778*

[b]*Key Laboratory of Environmental Biology and Pollution Control, Hunan University, Ministry of Education, Changsha 410082, Hunan, PR China*

† Electronic supplementary information (ESI) available. See DOI: 10.1039/c3an36928e

considerable attention as catalyst supports due to their extremely ordered and uniform pore structure, excellent electrocatalytic activity, high specific surface area and biocompatibility.[15] The uniform ordered porous structure provides a more favorable path for electrolyte penetration and transportation. The high surface area of the OMCs allows the high metal dispersion to be obtained, while biocompatibility of the OMCs result in the relative stability and bioactivity of the enzyme.[16] The structure of OMCs allows building blocks in hybrid materials, and provides an excellent platform for enzyme and protein immobilization. The introduction of noble metal nanoparticles can extend the application of OMCs and strengthens its features, such as catalytic and electrochemical activity.[17] Herein, Au nanoparticles (AuNPs) were introduced into OMCs. AuNPs are deemed as a good candidate due to the high effective surface area, nanoscaled dimensional effects, and good biocompatibility.[18] AuNPs also provide the protein molecules with more freedom of orientation and reduce the insulating effect of the protein shell for direct electron transfer.[19] AuNPs can be generally dispersed with a conducting support to avoid agglomeration and to keep their activities in practical applications. Herein, the OMCs were exploited as the support for AuNPs benefiting from the following advantages and features, higher affinity for the enzyme, larger bioactivity after entrapment procedures, and faster electron transfer between the enzyme and OMC-sensing sites. A film of AuNPs was immobilized on the electrode surfaces, to facilitate electron transfer through the conducting tunnels of colloidal gold.[19] Assembling AuNPs on an amino or thiol group-modified membrane is a common method in nano gold immobilization.[20,21] Herein, in the self-assembly process, L-lysine is able to provide an amino group and therefore becomes the cross-linking agent between AuNPs film and OMC–Au film. This effectively facilitates large loading of enzyme, makes the tyrosinase fix better on the biosensor, accelerates electron transfer from the enzyme-catalysed redox reaction to electrode surface, and extends its useful life.

In this work, OMC–Au nanocomposites were synthesized by a one-step chemical reduction route, and then a OMC–Au/L-lysine/Au composite film-modified GCE was newly constructed. Tyrosinase was then immobilized onto OMC–Au/L-lysine/Au/GCE to fabricate the biosensor. The biosensor was successfully used for simultaneous determination of HQ and CC. Moreover, DPV was performed to investigate the relationship between the peak current and the concentration of two dihydroxybenzene isomers. Compared with amperometry, DPV was considered as a better choice for the simultaneous detection of CC and HQ in real samples.

Experimental

Apparatus and reagents

Pluronic copolymer P123 (non-ionic triblock copolymer, $EO_{20}PO_{70}EO_{20}$) and tyrosinase (EC 1.14.18.1, from mushroom as lyophilized powder) were purchased from Sigma-Aldrich (USA). Tetraethoxysilane (TEOS), L-lysine, gold(III) chloride trihydrate ($HAuCl_4 \cdot 3H_2O$, 99.9%) and all other chemicals were of analytical grade and used as received. Phosphate buffer solutions (1/15 M PBS) with different pH were prepared by mixing the stock solution of NaH_2PO_4 and Na_2HPO_4. All solutions were prepared with doubly distilled water.

Cyclic voltammetric measurement and differential pulse voltammetric measurement were carried out on CHI660B electrochemical system (Chenhua Instrument, Shanghai, China). The three-electrode system used in this work consists of tyrosinase/OMC–Au/L-lysine/Au/GCE as the working electrode, a saturated calomel electrode (SCE) as the reference electrode and a Pt foil auxiliary electrode. All the work was conducted at room temperature (25 °C) unless otherwise stated. Scanning Electron Microscopy (SEM) was carried out by JSM-6360LV scanning electron microscope (JEOL Ltd, Japan). Transmission electron microscopy (TEM) images were performed on a JEOL-1230 electron microscope (JEOL, Japan) operated at 100 kV. X-ray diffraction (XRD) patterns were obtained on an X-ray D/max-2200 vpc (Rigaku Corporation, Japan) instrument operated at 40 kV and 20 mA, using Cu Kα radiation ($\lambda = 0.15406$ nm). Model PHSJ-3F laboratory pH meter (Leici Instrument, Shanghai, China) was used to test pH. A Sigma 4K15 laboratory centrifuge, a vacuum freezing dryer, and a mechanical vibrator were used in the assay.

Preparation of OMC and OMC–Au nanocomposites

The mesostructured SBA-15 silica template was synthesized following the reported method.[22] OMC was synthesized using SBA-15 as a template, and sucrose was used as a carbon source according to the method reported by Ryoo and co-workers[23] with slight alterations. A typical procedure was carried out as follows: 1 g of mesoporous silica material (SBA-15) was added to a solution obtained by dissolving 1.25 g of sucrose and 0.14 g of H_2SO_4 in 5 g of water. The mixture was placed in a drying oven for 6 h at 100 °C, and subsequently the oven temperature increased to 160 °C for another 6 h. To obtain fully polymerized and carbonized sucrose inside the pores of the silica template, the silica sample was treated again at 100 °C and 160 °C using the same drying oven after the addition of the same amount of sucrose, H_2SO_4 and H_2O. After the second sucrose addition, carbonization was performed under a 5% H_2–95% Ar atmosphere at 900 °C for 2 h with a heating rate of 2 °C min^{-1}. The product was washed with heated 3 M NaOH solution to remove the silica template, filtered, washed with distilled water, dried at 70 °C, and stored for further experiments.

OMC–Au nanocomposites were synthesized by a one-step reaction with $NaBH_4$ as reductant and sodium citrate as stabilizer in aqueous solution. The prepared OMC (4 mg) was suspended in 0.1 wt% $HAuCl_4$ solution (200 mL) by sonication for 10 h to obtain a good quality dispersed solution. Then 2 mL 1 wt% sodium citrate was added to the suspended solution while stirring. After 1 min, freshly prepared 2 mL 0.075 wt% $NaBH_4$ in 2 mL 1 wt% sodium citrate was quickly added to the solution under vigorous stirring. The reaction continued for 45 min until the color of the solutions did not change at room temperature. The black solid was separated by centrifuging at 4000 rpm, washed several times with deionized water and dried overnight in an oven at 80 °C.

Fabrication of tyrosinase/OMC–Au/L-lysine/Au/GCE

The bare GCE was polished carefully before each experiment with 1, 0.3 and 0.05 μm alumina powder, rinsed thoroughly with doubly distilled water between each polishing step and air-dried. The as-prepared OMC–Au nanocomposites (1 mg) were dispersed into 2 mL dimethylformamide (DMF) and the mixture was sonicated for 1 h to form a stable black suspension. The preparation of tyrosinase/OMC–Au/L-lysine/Au was carried out as follows: AuNPs were immobilized on pretreated glassy carbon by cyclic voltammetry (CV) in 0.1% $HAuCl_4$ between −0.8 and 1.0 V at 40 mV s^{-1}, then washed successively with water. The Au/GCE was scanned by CV in 1.0×10^{-3} M L-ysine between −0.8 and 1.0 V at 50 mV s^{-1} until a steady state was reached, then L-lysine/Au/GCE was washed with doubly distilled deionized water and dried in air. OMC–Au/L-lysine/Au/GCE was prepared by casting 5.0 μL of the OMC–Au suspension onto the surface of the L-lysine/Au/GCE, it was then washed with water and dried in air before use. Finally, 7.0 μL of the tyrosinase (2 mg mL^{-1}, 1/15 MPBS (pH 6.98)) was dropped onto the electrode surface and kept at 4 °C in a refrigerator for about 12 h and then the enzyme electrode was fabricated. Schematic diagram Scheme 1 presents the preparation of the tyrosinase biosensor. When not in use the enzyme electrode was stored in a moist state at 4 °C.

Sample preparation and measurement procedures

Under optimal conditions, CV was performed in 10.0 mL of 1/15 M PBS (pH 6.98) containing single or mixed components and CV was performed between −0.6 and +0.8 V at scan rate of 50 mV s^{-1}. The determination of hydroquinone or catechol in the samples was carried out using differential pulse voltammetry (DPV) from +0.6 to −0.2 V, with pulse amplitude of 0.05 V, pulse width of 0.05 s, and pulse period of 0.2 s.

Results and discussion

Characterization of the composite membrane on the electrode

SEM images of OMC, OMC–Au/L-lysine/Au/GCE, TEM images of OMC and OMC–Au are shown in Fig. 1. From Fig. 1A, it can be seen that OMC is made up of carbon nanorods that are evenly dispersed on the surface of GCE. Morphological and structural studies of OMC nanoparticles were performed by transmission electron microscope (TEM). The OMC clearly exhibits highly ordered carbon nanowires (Fig. 1C). Compared with Fig. 1C, well-dispersed Au nanoparticles (Fig. 1D) are observed on outer surface of OMC, and the diameter of AuNPs is about 4.5 nm. It should be noted that the ordered structure is not obviously affected by the presence of AuNPs, and Au nanoparticles are uniformly dispersed on the OMC. Fig. 1B presents the SEM image of OMC–Au/L-lysine/Au/GCE composite. It can be seen in the bottom of the window, the AuNPs, OMC–Au and L-lysine respectively covered above the gold nanocomposites.

The crystalline structure and the phase composition of OMC and OMC–Au were characterized by X-ray diffraction (XRD). Curve Fig. 2b shows a typical XRD pattern of the synthesized OMC–Au nanoparticle. Compared with the XRD analysis of OMC (Fig. 2a), the OMC–Au nanocomposites (Fig. 2b) show five peaks assigned to crystalline plane diffraction (1 1 1), (2 0 0),

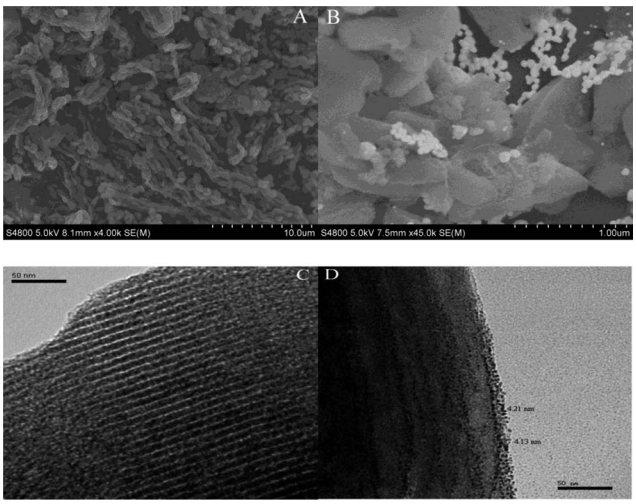

Fig. 1 (A) SEM image of OMC. (B) SEM image of OMC–Au/L-lysine/Au/GCE composite. (C) TEM image of OMC. (D) TEM image of OMC–Au.

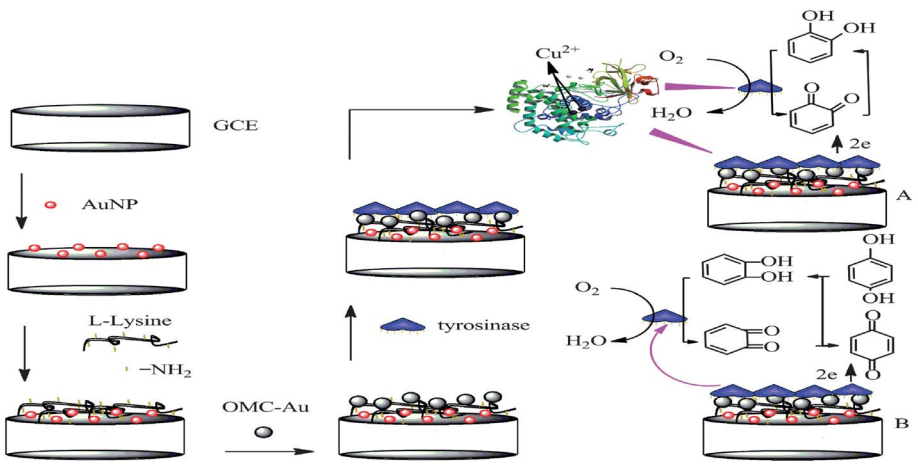

Scheme 1 Schematic diagram of the preparation of the tyrosinase biosensor. The proposed mechanism of the tyrosinase biosensor for HQ (B) and CC (A) electrocatalytic detection.

(2 2 0), (3 1 1), and (2 2 2) for the AuNPs, indicating evident face-centered cubic (fcc) Au crystal structure nanocomposites (JCPDF04-0784).

Electrochemical behavior of the electrode

Electrochemical impedance spectroscopy (EIS) of $[Fe(CN)_6]^{3-/4-}$ can provide information about the impedance changes of the electrode surface during the modification process. The interface can be modeled by an equivalent circuit. This equivalent circuit includes the electron-transfer resistance (R_{ct}), the Warburg impedance (Z_w), the ohmic resistance of the electrolyte (R_s), and interfacial capacitance (C_{dl}). EIS includes a semicircular part and a linear part. The semicircle diameter represents the electron-transfer resistance, R_{et}, which dominates the electron transfer kinetics of the redox probe at the electrode interface. Meanwhile, the linear part at lower frequencies correspond to the diffusion process.[24] Fig. 3 displays the EIS results of the different modified electrodes, which were fitted based on the equivalent circuit (Fig. 3, inset). The interfacial electron-transfer resistance (R_{et}) for bare GCE was 1269.25 Ω. After modification of Au nanoparticles, the value of R_{et} decreased to 156.25 Ω, indicating that the introduction of AuNPs could improve electron transfer kinetics to a large extent in the self-assembly process of the biosensor (curve GCE/Au). Then, the value of R_{et} increased to 237.45 Ω after the introduction of L-lysine (curve GCE/Au/L-lysine). The reason for this is the non-conductivity of the L-lysine component in the film. Although the L-lysine film did not increase electrical conductivity or the rate of electron transfer, and had no catalytic effect in the construction of the biosensor, it did make the AuNPs film and OMC–Au film fix more tightly to the substrate through the amino group as a molecular bridge. This method might extend the useful life and stability of the biosensor. An almost straight line was observed for the assembly of OMC–Au on the modified GCE (curve GCE/Au/L-lysine/OMC–Au), indicating that the introduction of OMC–Au can improve the electron transfer kinetics to a large extent. Moreover, an obvious increase in the interfacial resistance was observed when tyrosinase was entrapped in the OMC–Au film. The value of R_{et} was increased to 914.04 Ω (curve GCE/Au/L–lysine/OMC–Au/tyrosinase). Such increased R_{et} can be ascribed to entrapment and low conductivity of the tyrosinase, which slowed the redox reaction of $[Fe(CN)_6]^{3-/4-}$. Finally, it was observed that adsorption of tyrosinase onto OMC–Au is related to the decrease of the semicircle, indicating that tyrosinase has been successfully immobilized onto the GCE modified with OMC–Au.

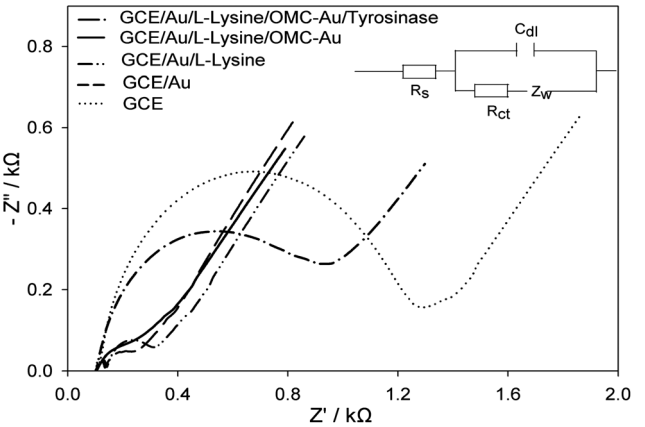

Fig. 3 Electrochemical impedance spectra of GCE/Au/L-lysine/OMC–Au/tyrosinase, GCE/Au/L-lysine/OMC–Au, GCE/Au, GCE/Au/L-lysine and GCE, using a 0.1 M KCl solution containing 5.0 mM ferro/ferricyanide, with frequency range of 0.1–10^5 Hz, a bias potential of 0.19 V *vs.* SCE and an AC amplitude of 5 mV.

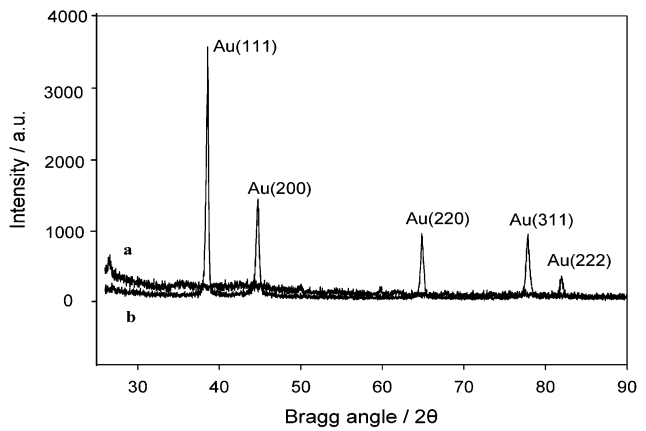

Fig. 2 D patterns of OMC (a) and OMC–Au (b).

Catalytic reaction mechanism of the biosensor

Tyrosinase (or polyphenol oxidase) catalysed the oxidation and hydroxylation of monophenols, diphenols, aromatic amine, *etc.* The redox reaction of hydroquinone and catechol catalysed by tyrosinase is described as follows:

$$CC + O_2 \xrightarrow{\text{tyrosinase}} o\text{-quinone} + 2H_2O \quad (1)$$

$$HQ + O_2 \xrightarrow{\text{tyrosinase}+o\text{-quinone}} 1,4\text{-benzoquinone} + 2H_2O \quad (2)$$

$$o\text{-quinone(1,4-benzoquinone)} + 2e + 2H^+ \rightarrow CC(HQ) \quad (3)$$

Tyrosinase can catalyze the oxidation of catechol to *o*-quinone (eqn (1)). Hydroquinone is not a primary substrate for the enzyme, but is vicariously oxidized in the presence of tyrosinase and *o*-quinone (eqn (2)).[13] Under optimized conditions, *o*-quinone and 1,4-benzoquinone may be electrochemically reduced to CC and HQ (eqn (3)). The oxidation process by the tyrosinase, followed by reduction at the electrode surface, may yield a catalytically amplified current. Therefore, at the electrode surface reduction of *o*-quinone to catechol and 1,4-benzoquinone to hydroquinone (as the working electrode) acts as the cathode.

Scheme 1 shows GCE/Au/L-lysine/OMC–Au and the proposed mechanism for HQ and CC electrocatalytic detection using the OMC–Au based biosensor. Tyrosinase is a multicopper phenol oxidase. It can oxidize hydroquinone, catechol and utilize dioxygen as an oxidant, reducing it to water. In the reaction, hydroquinone and catechol, as the electron donor for the

oxidized form of the enzyme, were mainly converted into 1,4-benzoquinone and *o*-quinone, and then reduced on the surface of the electrode.[25] This efficiently shuttled electrons between tyrosinase redox center and GCE/Au/L-lysine/OMC–Au surface in a dynamical equilibrium, leading to the detectable response current.

Optimization of experimental conditions

The effect of solution pH on the response of CC and HQ at GCE/Au/L-lysine/OMC–Au/tyrosinase was investigated in the range of 4.5–9.2. The anodic peak currents for CC and HQ increased with pH from 4.5 to 6.98 (Fig. 4A), and reached a maximum value at pH 6.98. When the pH value is higher than 6.98, the peak current decreases rapidly. In addition, the relationship between pH and the anodic peak potential was investigated (Fig. 4B). It can be seen that the anodic peak potentials shift negatively with pH increasing from 4.2 to 9.2 for both CC and HQ. The two regression lines are almost parallel, indicating that the peak-to-peak separation between CC and HQ is constant at different pH solutions. The equations for peak potential with pH for CC and HQ are expressed as follows:

$$E_{CC} = 554.4 - 618.8\ \text{pH (mV, } r^2 = 0.9717) \quad (4)$$

$$E_{HQ} = 655.0 - 62\ \text{pH (mV, } r^2 = 0.9843) \quad (5)$$

The slopes of these equations are close to the theoretical value of 59 mV pH^{-1} for the two proton and two electron process,[26] suggesting that the redox reaction of CC (or HQ) at GCE/Au/L-lysine/OMC–Au/tyrosinase should be a two electrons and two protons process. Therefore, pH 6.98 was chosen as the optimum pH value for the detection of hydroquinone and catechol in order to achieve high sensitivity.

Fig. 5A shows CVs obtained at GCE in 0.1% $HAuCl_4$ at different scan rates. A series of well-defined quasi-reversible redox waves were observed at GCE in the potential range of 0.0 V and 1.6 V. Both the redox peak currents and the peak-to-peak difference increase with increasing scan rates. The significant increase of the redox peak currents when the potential scan rate is increased can result in a decrease of AuNPs on the electrode surface. Therefore, in order to achieve appropriate AuNPs, 50 mV s^{-1} was chosen as the optimum scan rate value for the immobilization of Au nanocomposites.

The relationship between the redox peak current response and the coverage of tyrosinase solution was investigated by cyclic voltammetry of 50 μM catechol in 1/15 M PBS solution. Fig. 5B displays the reduction peak responses which increase markedly with the coverage of tyrosinase from 8 to 24 μg cm^{-2}.

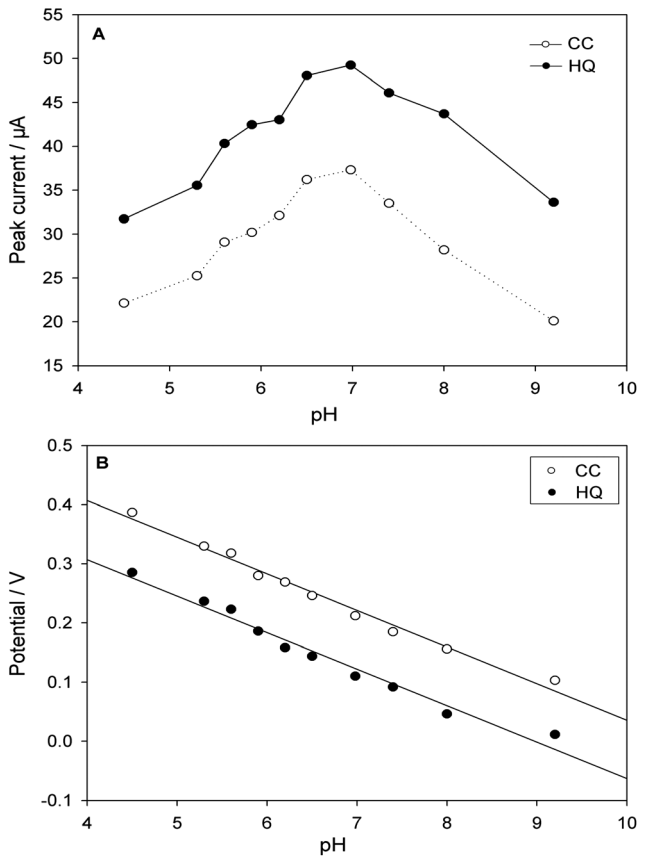

Fig. 4 Effect of pH on anodic peak current for CC (1×10^{-5} M) (A) and anodic peak potential for HQ (1×10^{-5} M) (B).

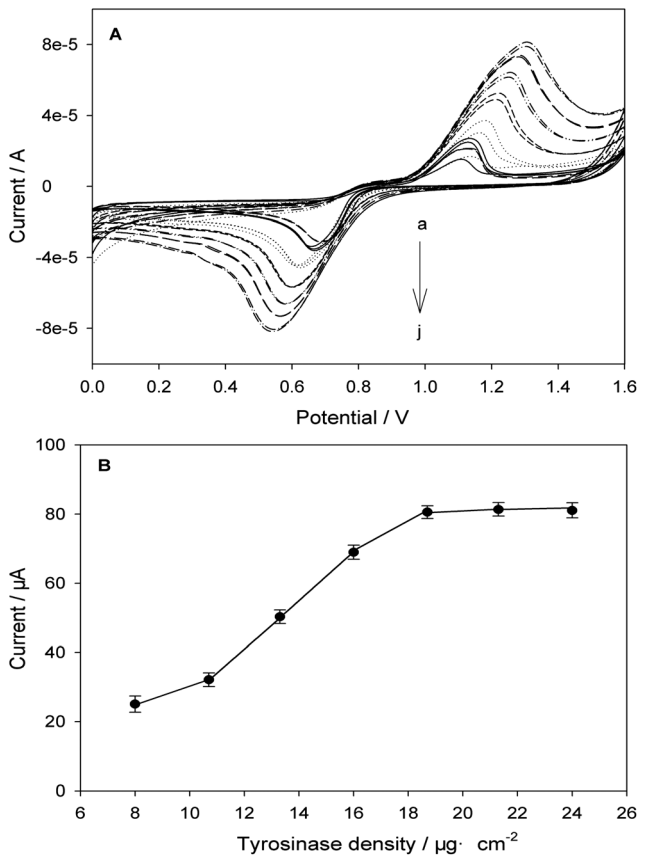

Fig. 5 (A) CVs acquired on GCE with 0.1% $HAuCl_4$ at different scan rates: a–j: 10, 20, 40, 60, 80, 100, 120 mV s^{-1}. (B) Optimization of the coverage of tyrosinase. The ordinates are presented as the reduction peak current by cyclic voltammetry of 50 μM catechol in 1/15 M PBS solution. The vertical bars designate the standard deviation of the means in three replicate tests.

However, upon further increasing the coverage of tyrosinase, the reduction peak current responses decreased slightly, for the thicker film of tyrosinase blocked the electrical conductivity. Thus, tyrosinase coverage with 18.67 μg cm^2 (7.0 μL, 2 mg mL^{-1}) was employed to modify the electrode.

Electrode response characteristics

DPV was performed to investigate the relationship between the peak current and concentration of HQ and CC due to its higher sensitivity. The utilization of the GCE/Au/L-lysine/OMC–Au/tyrosinase for the simultaneous determination of HQ and CC was demonstrated by simultaneously changing their concentrations. The DPV results show two well distinguished DPV peaks at potentials of 24.79 and 160.64 mV, corresponding to the redox of HQ and CC, respectively (Fig. 6). When the peak-to-peak difference for CC, HQ was between 100 and 125 mV, it indicated that DPV could offer a special approach for simultaneous and sensitive electrochemical determination of dihydroxybenzene isomers in the mixture solution.[2,27–34] In this paper, the detected potential difference between HQ and CC was 135.85 mV, which was large enough for simultaneous determination of the concentrations of these two substances. A third small voltammetric peak was also observed, its peak potential has a certain distance to the peak potentials of hydroquinone and catechol, which are 115.48 mV, 251.33 mV, respectively. However, the small voltammetric peak made little change in the potentials or currents among tests of the blank sample and samples with different substrate concentrations during the experiment. Therefore, we conclude that this voltammetric peak has little influence on the simultaneous determination of hydroquinone and catechol. Thus, the isomers could be suitable for simultaneous determination at a modified GCE. A comparison of the proposed method with other electrochemical methods is listed in Table 1. It can be seen that many articles have been written about these topics, especially, sensors for the simultaneous determination of hydroquinone, catechol. However, a tyrosinase biosensor for the simultaneous determination of CC and HQ has not yet been reported. The peak separation is wider and the peak potential is lower than those of other reported sensors, which makes this biosensor an advantageous device for real sample applications.

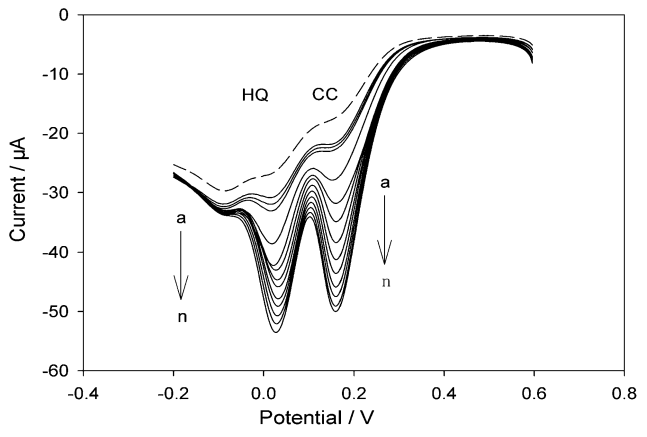

Fig. 6 Differential pulse voltammetry of various concentrations of HQ and CC both from 0 to 8×10^{-5} M in pH 6.98 PBS: (a) 0, (b) 4×10^{-7} M, (c) 5×10^{-7} M, (d) 6×10^{-7} M, (e) 1×10^{-6} M, (f) 2×10^{-6} M, (g) 4×10^{-6} M, (h) 6×10^{-6} M, (i) 8×10^{-6} M, (j) 1×10^{-5} M, (k) 2×10^{-5} M, (l) 4×10^{-5} M, (m) 6×10^{-5} M, (n) 8×10^{-5} M.

Fig. 7 shows the calibration of the concentrations of HQ and CC. As can be seen in Fig. 7A, under the optimal conditions, the cathodic peak current was linear with the logarithmic value of hydroquinone concentration ranging from 4×10^{-7} M to 8.0×10^{-5} M. The regression equation is $P_{HQ} = -66.954 - 9.5357\lg[HQ]$ (P_{HQ}: μA, [HQ]: M), and $R = 0.9565$. According to the generally accepted definition, the lower detection limit of HQ is 5×10^{-8} M, which resulted in a current signal that equals the mean value of background signals plus three times standard deviation of background signals. Similarly, as shown in Fig. 7B, the cathodic peak current of catechol increased with its concentration increasing from 4×10^{-7} M to 8.0×10^{-5} M. A linear regression equation was obtained as $P_{CC} = -88.394 - 13.081\lg[CC]$ (P_{CC}: μA, [CC]: M); ($R = 0.9771$), and the detection limit was 2.5×10^{-8} M. Each calibration was carried out three times with the standard deviations of current response not more than 3%. Compared with the recently reported tyrosinase-modified biosensors on different electrode substrates,[10,12,35–44] the proposed GCE/Au/L-lysine/OMC–Au/Tyr biosensor exhibited improved analytical performance in terms of linear range of response, as presented in Table 2. Although the detection limit was not significantly improved, the difference between peak potentials for hydroquinone and pyrocatechol is wide (135.85 mV) and both peak potentials are low. Thus, this assay provided the potential to quantify the CC and HQ levels in real environmental water samples.

All these results indicate that the developed OMC–Au based electrochemical biosensor is an excellent candidate for CC and HQ detection. This behavior might be explained by higher loading of tyrosinase because of efficient entrapping of the enzyme in the OMCs film,[16] and a decrease in the resistance of the biosensor upon the addition of OMC and Au nanoparticles into the membrane (Fig. 3). OMC–Au herein retained tyrosinase activity to a large extent after entrapping. Although the exact nature of the enzyme entrapment and electron transfer in OMC–Au on electrode surface has not been clearly defined, there is a hypothesis that the small size of AuNPs made the enzyme molecules more free in orientation and the prosthetic group closer to the particles surface.[18,19] In this work, the uniformly dispersed AuNPs on the OMC had very high surface energy, and may strongly act with tyrosinase molecules and increase the density of adsorption. They also may shorten the distance for electron transfer between the prosthetic group of tyrosinase containing copper and the OMC–Au surface, this was further enhanced by the AuNPs film on the electrode, and finally led to high sensitivity of the biosensor. The sensitivity trend was catechol > hydroquinone, and the difference in sensitivity might depend on the tyrosinase catalytic selectivity for different phenolic compounds. Catechol is a substrate of tyrosinase, while hydroquinone could act as secondary substrate.[13]

Table 1 Performance comparison of peak separation of hydroquinone and catechol with other fabricated electrodes

Electrode	Method	Peak potential (mV)		Peak separation (mV)	Ref.
		HQ	CC		
MWCNT[a]/GCE	CV	152	256	104	25
SWNT[b]/GCE	CV	157	268	111	26
Graphene/GCE	CV	207	319	112	27
Mesoporous Pt electrode	DPV	460	560	100	28
Graphene–chitosan/GCE	CV	53	153	100	2
MWCNT–ionic liquids–Gel/GCE	DPV	104	199	95	29
Poly(thionine)/GCE	DPV	130	230	100	30
Graphene sheet[c]/$BMIMPF_6$/GCE	CV	220	325	105	31
Electrospun carbon nanofibre/CPE[d]	DPV	—	—	110	32
Tyr/OMC–Au/L-lysine/Au/GCE	DPV	24.79	160.64	135.85	This work

[a] MWCNT: multi-wall carbon nanotubes. [b] Single-wall carbon nanotube. [c] $BMIMPF_6$: 1-butyl-3-methylimidazolium hexafluorophosphate. [d] CPE: carbon paste electrode.

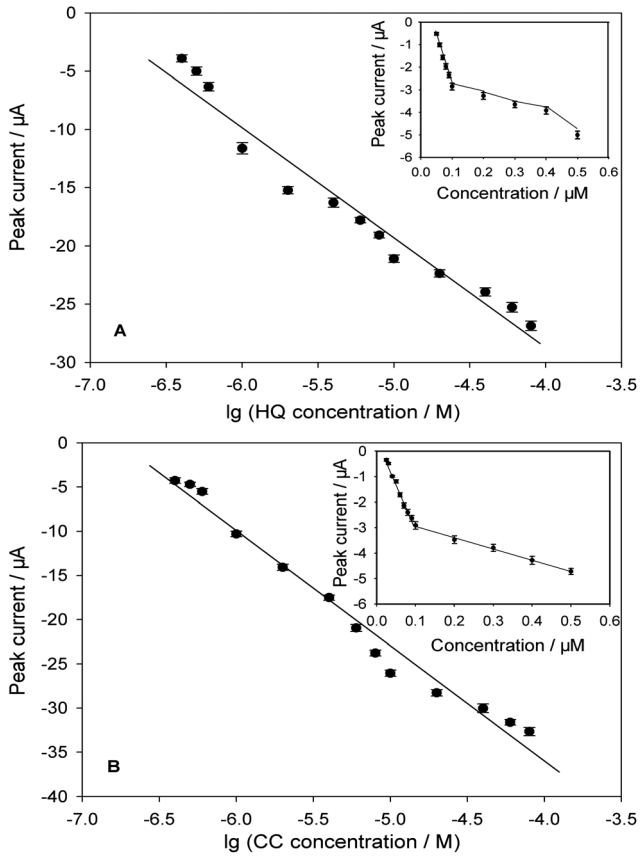

Fig. 7 (A) Calibration plot of HQ concentration in PBS (1/15 M, pH 6.98). (Inset) The plot of peak current *vs.* HQ concentration between 0.05 and 0.5 μM. (B) Calibration plot of CC concentration in PBS (1/15 M, pH 6.98). (Inset) The plot of peak current *vs.* CC concentration between 0.025 and 0.5 μM.

Reproducibility and stability of the biosensor

The repeatability of the same GCE/Au/L-lysine/OMC–Au/tyrosinase biosensor was examined by detecting 50 μM catechol in 1/15 M PBS using DPV. A relative standard deviation (R.S.D.) value of 2.9% was obtained for five successive determinations, which implied good repeatability of the measurements with no need to apply a complicated pretreatment procedure to the electrode. The reproducibility was also investigated with five different GCEs constructed by the same steps independently, as presented in Fig. S1 (ESI†). The RSD was 3.2% for the response current to 50 μM catechol, indicating that the fabrication procedure was reliable and the modified GCE had good reproducibility.

The long-term stability of the biosensor was explored. It was investigated through the response to 50 μM catechol in 1/15 M PBS for 1 month. When not in use, electrode was stored at 4 °C in a refrigerator, and the current response was periodically measured. Beyond this period, the experiment was carried out per 10 days. The result showed that the biosensor retained about 85% of its original response after 1 month. The relatively good stability of the biosensor may be explained by the fact that the film can provide a biocompatible microenvironment and the specific ability of tyrosinase can be protected effectively.

Analysis of water samples

To evaluate the practicality of the present method, the biosensor was applied to simultaneously detect the recoveries of CC and HQ in tap water. The results were calculated from the standard calibration curves in Fig. 7. It is observed that the average recoveries of CC range from 98.08% to 105.73%, and those of HQ range from 98.08% to 105.73% for the real samples.The relative signal deviation is not more than 4.5%, as presented in Table S1 (ESI†). Thus these satisfactory results confirmed the potential applicability of the biosensor for the quantification of CC and HQ.

Interference

Fig. S2 (ESI†) shows the effect of interferents on the tyrosinase biosensor for catechol. The first bar shows the current change obtained from 1×10^{-5} M catechol. The remaining bars show the current change for the mixture of catechol (1×10^{-5} M) and interferents (1×10^{-5} M). CC and 1, 2, 3, 4, 5, 6 stand for catechol, hydroquinone, phenol, guaiacol, 3,5-dinitrosalicylic acid, *N*,*N*-dimethylaniline, and glucose, respectively. The degree

Table 2 A comparison of analytical characteristics towards catechol for tyrosinase biosensors reported in the literature

		Linear range ($\times 10^{-6}$ mol L^{-1})		LOD ($\times 10^{-6}$ mol L^{-1})		
Electrode	Method	HQ	CC	HQ	CC	Ref.
Tyr[a]–silicate–Nafion/GCE	i-t		1–100		0.35	33
Tyr–copolymer poly-indium-tin-oxide(ITO) coated glass plate.	i-t		1.6–118.8		1.20	34
Tyr layer-by-layer immobilized on latex particles	i-t		2–19.7		—	35
Tyr entrapped in polyacrylamide microgels	i-t		0.5–24		0.30	36
Tyr immobilized within Os-complex Functionalized electrodeposition polymer	i-t		—		0.01	37
Tyr-Au_{coll}–graphite–Teflon	i-t		0.01–8		0.02	38
Tyr immobilized on a sonogel–carbon matrix	i-t		—		0.064	39
Tyr/CoPc[b]/CGCE[c]	i-t		3–863		0.45	40
Tyr–Fe_3O_4–chitosan/GCE	i-t	—	0.083–70	—	0.025	10
Tyr–Al_2O_3 modified sonogel carbon electrode.	i-t	—	0.1–30	—	0.03	41
Tyr–Au/PASE–GO[d]/SPE[e]	i-t		0.083–23	0.076	0.024	12
BiNPs[f]/Tyr/SPE			0.5–100		0.062	42
Au/L-lysine/OMC–Au/Tyr/GCE	DPV	0.4–80	0.4–80	0.05	0.025	This work

[a] Tyr: tyrosinase. [b] CoPc: cobalt(II) phthalocyanine. [c] CGCE: acetylcellulose-graphite composite. [d] PASE-GO: succinimidyl ester-graphene oxide. [e] SPE: screen printed electrode. [f] BiNPs: bismuth nanoparticles.

of interference is calculated according to the following equation:

$$\tau = \frac{|I_0 - I_N|}{I_0} \quad (6)$$

where τ is the percent of interference; I_0 and I_N stand for the response currents to 1×10^{-5} M catechol and interferent, respectively. Due to the slight decreasing of *o*-quinone as the hydroquinone is oxidized (eqn (2)), the current of catechol by adding the same amount of hydroquinone is reduced (the second bar) and the maximum relative response current change increased to 2.293% for hydroquinone. The third, fourth bars show that the currents are lessened compared with catechol (the first bar), which may be attributed to the slight increasing of *o*-quinone as the phenol and guaiacol were oxidized. However, the relative responses obtained from most of these interferents are found to be negligible (<2.293%). Therefore, the proposed tyrosinase biosensor exhibits the ability to reduce the influences of possible interferences and can be used to selectively determine catechol and hydroquinone without interference, which may be ascribed to the very wide peak separation and low peak potential.

Conclusion

In this work, a novel tyrosinase biosensor, using differential pulse voltammetry (DPV), for simultaneous determination of dihydroxybenzene isomers is proposed. The biosensor was developed based on tyrosinase immobilization with OMC–Au, L-lysine membrane and AuNPs, which to our knowledge has not previously been reported. In the fabrication of the tyrosinase biosensor, the nano-biocomposite film provided a suitable microenvironment, which could effectively present a large loading amount of enzyme and so prevent the leaching of the immobilized enzyme, and dihydroxybenzene isomers efficiently shuttles electrons between tyrosinase redox center and GCE surface. The DPV results showed that the peak potential difference between hydroquinone and pyrocatechol is wide (135.85 mV) and peak potentials are low. The optimized experimental conditions for the operation of the enzyme biosensor were studied and the response mechanism of the OMC based on electrochemical was discussed. The resulting biosensor exhibited a good analytical performance for the DPV detection of HQ and CC without extra mediators, and showed high sensitivity, low detection limit, good selectivity and stability. The proposed strategy can be extended for the development of other enzyme-based biosensors.

Acknowledgements

The study was financially supported by Program for the Outstanding Young Talents of China, the National Natural Science Foundation of China (51222805), the Program for New Century Excellent Talents in University from the Ministry of Education of China (NCET-11-0129), the Fundamental Research Funds for the Central Universities, Hunan University, Foundation for the Author of Excellent Doctoral Dissertation of Hunan Province, and Hunan Provincial Innovation Foundation For Postgraduate (CX2009B080).

References

1 J. Wang, J. N. Park, X. Y. Wei and C. W. Lee, *Chem. Commun.*, 2003, 628–629.
2 Y. Zhang, G. M. Zeng, L. Tang, D. L. Huang, X. Y. Jiang and Y. N. Chen, *Biosens. Bioelectron.*, 2007, **22**, 2121–2126.
3 L. H. Wang and Y. P. Kuo, *Chromatographia*, 1999, **49**, 208–211.
4 J. A. G. Mesa and R. Mateos, *J. Agric. Food Chem.*, 2007, **55**, 3863–3868.
5 M. F. Pistonesi, M. S. D. Nezio, M. E. Centurion, M. E. Palomeque, A. G. Lista and B. S. F. Band, *Talanta*, 2006, **69**, 1265–1268.
6 P. Nagaraja, R. A. Vasantha and K. R. Sunitha, *J. Pharm. Biomed. Anal.*, 2001, **25**, 417–424.
7 J. J. Yu, W. Du, F. Q. Zhao and B. Z. Zeng, *Electrochim. Acta*, 2009, **54**, 984–988.
8 R. Kazandjian and A. Klibanov, *J. Am. Chem. Soc.*, 1985, **107**, 5448–5450.
9 J. J. Berenguer, A. Manjon and J. L. Iborra, *Bioresour. Technol.*, 1989, **3**, 211–216.
10 S. F. Wang, Y. M. Tan, D. M. Zhao and G. D. Liu, *Biosens. Bioelectron.*, 2008, **23**, 1781–1787.
11 G. Alarcon, M. Guix, A. Ambrosi and M. T. R. Silva, *Nanotechnology*, 2010, **21**, 245502–245510.
12 W. Song, D. W. Li, Y. T. Li, Y. Li and Y. T. Long, *Biosens. Bioelectron.*, 2011, **26**, 3181–3186.
13 M. R. L. Stratford, C. A. Ramsden and P. A. Riley, *Bioorg. Med. Chem.*, 2012, **20**, 4364–4370.
14 B. Haghighi and M. A. Tabrizi, *Electrochim. Acta*, 2011, **56**, 10101–10106.
15 M. Zhou, L. Shang, B. L. Li, L. J. Huang and S. J. Dong, *Biosens. Bioelectron.*, 2008, **24**, 442–447.
16 Y. Y. Liu, Z. T. Zeng, G. M. Zeng, L. Tang, Y. Pang, Z. Li, C. Liu, X. X. Lei, M. S. Wu, P. Y. Ren, Z. F. Liu, M. Chen and G. X. Xie, *Bioresour. Technol.*, 2012, **115**, 21–26.
17 X. J. Bo, J. Bai, B. Qin and L. P. Guo, *Biosens. Bioelectron.*, 2011, **28**, 77–83.
18 L. X. Wang, J. Bai, X. J. Bo, X. L. Zhang and L. P. Guo, *Talanta*, 2011, **83**, 1386–1391.
19 S. Q. Liu, D. Leech and H. X. Ju, *Anal. Lett.*, 2003, **36**, 1–19.
20 C. Humbert, B. Busson, J. P. Abid, *et al.*, *Electrochim. Acta*, 2005, **50**, 3101–3110.
21 S. Kumar and S. Z. Zou, *Langmuir*, 2007, **23**, 7365–7371.
22 D. Y. Zhao, J. L. Feng, Q. S. Huo, *et al.*, *Science*, 1998, **279**, 548–552.
23 S. Jun, S. H. Joo, R. Ryoo, M. Kruk, M. Jaroniec, Z. Liu, T. Ohsuna and O. Terasaki, *J. Am. Chem.Soc.*, 2000, **122**, 10712–10713.
24 P. Du, H. X. Li, Z. H. Mei and S. F. Liu, *Bioelectrochemistry*, 2009, **75**, 37–43.
25 L. Tang, G. M. Zeng, J. X. Liu, X. M. Xu, Y. Zhang, G. L. Shen, Y. P. Li and C. Liu, *Anal. Bioanal. Chem.*, 2008, **391**, 679–685.
26 S. H. D. Vall and R. L. M. Creery, *Anal. Chem.*, 1999, **71**, 4594–4602.
27 Y. P. Ding, W. L. Liu, Q. S. Wu and X. G. Wang, *Electroanal. Chem.*, 2005, **575**, 275–280.
28 Z. H. Wang, S. J. Li and Q. Z. Lv, *Sens. Actuators, B*, 2007, **127**, 420–425.
29 H. J. Du, J. S. Ye, J. Q. Zhang, X. D. Huang and C. Z. Yu, *J. Electroanal. Chem.*, 2011, **650**, 209–213.
30 M. A. Ghanem, *Electrochem. Commun.*, 2007, **9**, 2501–2506.
31 C. H. Bu, X. H. Liu, Y. J. Zhang, L. Li, X. B. Zhou and X. Q. Lu, *Colloids Surf., B*, 2011, **88**, 292–296.
32 A. J. S. Ahammad, M. M. Rahman, G. R. Xu, S. Kim and J. J. Lee, *Electrochim. Acta*, 2011, **56**, 5266–5271.
33 Z. M. Liu, J. H. Wang, Y. Y. Cao, Y. F. Jing and Y. L. Liu, *Sens. Actuators, B*, 2011, **157**, 540–546.
34 Q. H. Guo, J. S. Huang, P. Q. Chen, Y. Liu, H. Q. Hou and T. Y. You, *Sens. Actuators, B*, 2012, **163**, 179–185.
35 M. A. Kim and W. Y. Lee, *Anal. Chim. Acta*, 2003, **479**, 143–150.
36 W. Rajesh, K. Takashima and K. Kaneto, *Sens. Actuators, B*, 2004, **102**, 271–277.
37 P. Rijiravanich, K. Aoki, J. Chen, W. Surareungchai and M. Somasundrum, *Electroanal. Chem.*, 2006, **589**, 249–258.
38 J. P. H. Pérez, M. S. P. López, E. L. Cabarcos and B. L. Ruiz, *Biosens. Bioelectron.*, 2006, **22**, 429–439.
39 H. B. Yildiz, J. Castillo, D. A. Gushin, L. Toppare and W. Schumann, *Microchim. Acta*, 2007, **159**, 27–34.
40 V. Carralero, M. L. Mena, A. G. Cortés, P. Y. Sedeño and J. M. Pigarrón, *Biosens. Bioelectron.*, 2006, **22**, 730–736.
41 M. E. I. Kaoutit, I. N. Rodriguez, K. R. Temsamani and J. L. H. H. Cisneros, *Biosens. Bioelectron.*, 2007, **22**, 2958–2966.
42 D. Yaico, T. Albuquerque and L. F. Ferreira, *Anal. Chim. Acta*, 2007, **596**, 210–221.
43 H. Zejli, J. L. H. H. Cisnerosc, I. N. Rodriguezc, B. Liu, K. R. Temsamanib and J. L. Marty, *Anal. Chim. Acta*, 2008, **612**, 198–203.
44 C. Carmen, M. Martinez, M. Cadevall, M. Guix, J. Ros and A. Merkoci, *Biosens. Bioelectron.*, 2013, **40**, 57–62.